Titanium with controllable pore fractions by thermoreversible gelcasting of TiH$_2$

Kendra A. Erk, David C. Dunand, Kenneth R. Shull *

Department of Materials Science and Engineering, Northwestern University, 2220 Campus Drive, Evanston, IL 60208, USA

Abstract

Thermoreversible gelcasting, a near-net-shape processing technique, is demonstrated here for titanium. The gelcasting system is composed of TiH$_2$ particles suspended in a triblock copolymer gel that behaves as a viscous liquid above 56 °C and an elastic solid at room temperature, a temperature-dependent transition that is fully reversible when solvent is present. Organic pyrolysis to remove the gel followed by vacuum sintering to densify the Ti powders (produced by decomposition of the hydride) results in titanium with near full density and low contamination. Incorporation of polypropylene and poly(methyl methacrylate) space-holder particles into the gel results in titanium with controlled porosities up to 44 vol.% and with low contamination. These foams exhibit tailorable stiffness and strength, together with excellent compressive ductility and energy absorption.
© 2008 Acta Materialia Inc. Published by Elsevier Ltd. All rights reserved.

Keywords: Porous material; Powder processing; Titanium hydride; Foams; Mechanical properties

1. Introduction

Porous titanium is an exceptional material for specialized structural applications [1]. Commercially pure titanium fulfills important chemical and mechanical requirements for use in medical implants as it exhibits a higher specific strength, lower stiffness, and improved corrosion resistance in biological media as compared with stainless steel and cobalt–chromium alloys [2–5]. The incorporation of porosity into titanium implants provides additional advantages over fully dense titanium: mechanical anchoring to bone is facilitated through tissue growth into the pores and stiffness is reduced, thus mitigating stress shielding [5]. Porous titanium is also an attractive candidate for heat exchangers and condensers as the thermal conductivity of titanium is 50% higher than stainless steel [6]. Porous titanium and Ti-based sandwiches are additionally used for vibrational damping and energy-absorbing structures, supports for catalysts, filtration systems, and lightweight construction [7–10].

There is a general need for an easier fabrication route for dense titanium components, as compared to the traditional processing routes: (1) liquid metallurgy (vacuum casting, forging, and machining to desired specifications) or (2) powder metallurgy (powder compaction, vacuum sintering with or without pressure, and machining) [2,3,6,11]. Near-net-shape processing techniques to create dense titanium structures with complex shapes, such as investment casting, precision forging, and hot-die forging, require high temperatures and pressures and may result in contamination [12]. Titanium with tailored porosity can be produced by various techniques, some of which include powder sintering to achieve partial densification [5,13,14], sintering with the addition of temporary space-holders [15–19], and pressurized pore expansion with argon or hydrogen gas [20,21]. To form complex shapes of porous titanium, machining of the consolidated greenbody or sintered component must be performed [15,22].

Conventional gelcasting, a near-net-shape ceramic processing technique [23,24], has been previously applied to

---

* Corresponding author. Tel.: +1 847 467 1752.
E-mail address: k-shull@northwestern.edu (K.R. Shull).

ceramics [23,25–28] but rarely to metals (e.g. nickel-based superalloy [29], steel [30,31], and copper [32]). In this technique, ceramic or metal powders, organic binders (i.e. monomer), dispersant, and solvent are mixed to form a low-viscosity slurry. Prior to casting, initiator and catalyst molecules are added to the mixture in concentrations that permit pouring of the slurry into the mold before subsequent formation of a chemically crosslinked, polymer–solvent network (i.e. gel) by free radical polymerization. The gel assumes the shape of the mold and suspends the ceramic/metal particles. After solvent evaporation, the polymer acts to bind the particles and retain the desired shape. Finally, the polymer binder is pyrolyzed, and the particles are sintered to form a dense ceramic or metal structure.

Thermoreversible gelcasting involves the formation of a reversible, physically crosslinked polymer gel as opposed to the permanent, chemically crosslinked gel formed in conventional gelcasting. The gel is composed of triblock copolymer, such as poly(methyl methacrylate)–poly(n-butyl acrylate)–poly(methyl methacrylate) (PMMA–PnBA–PMMA, see Fig. 1), in a solvent that preferentially dissolves the midblock (PnBA). At high temperatures, the triblock copolymer is fully dissolved in the solvent, forming a free-flowing, low-viscosity liquid as illustrated in Regime 1 of Fig. 1. Below a critical temperature termed the critical micelle temperature (CMT; i.e. order–disorder transition), the PMMA endblocks self-assemble into spherical micelles or aggregates [33]. As shown in Regime 2 of Fig. 1, the PMMA aggregates act as physical crosslinks interconnected by PnBA "bridges" in a solvent matrix, resulting

in the formation of a viscoelastic liquid [34]. As the gel is cooled below the glass transition temperature (T_g) of the partially solvated PMMA endblocks (i.e. cooling from Regime 2 to Regime 3), the physical structure of the network remains unchanged. However, the exchange rate of PMMA endblocks between neighboring aggregates diminishes, and a strong, elastic solid is formed. The overall transition from an initial low-viscosity liquid (Regime 1) to an elastic network (Regime 3) is best defined by the gel temperature. For the system investigated here, the gel temperature is close to 60 °C and exists in the temperature range of Regime 2, between the CMT and T_g [34,35].

The thermoreversible nature of the triblock copolymer gel allows the gel to act as a fluid casting medium at high temperatures for solid particles (Regime 1; e.g. 65–80 °C) and as an organic binder between the solid particles at low temperatures (Regime 3; e.g. room temperature) [36]. In the low-viscosity liquid regime at elevated temperatures, particles are added to the solution, and the mixture is poured into a mold. After cooling below the gel temperature to room temperature, the particles are suspended by the elastic polymer network; this is depicted, approximately to scale, in Regime 3 of Fig. 1 for micron-sized titanium hydride particles. The cooled particle-filled gel is able to maintain its shape when removed from the mold. In a closed environment where solvent evaporation is minimized, the gelled structure can be reheated to a liquid and recast multiple times. After drying (i.e. solvent evaporation), the polymer binder is removed by low-temperature pyrolysis, subsequently followed by high-temperature sintering of the solid particles to form a dense object. Porous objects can be fabricated with the addition of organic space-holder particles to the gelcasting slurry.

Past studies have focused on thermoreversible gelcasting of ceramic particles [37,38]. The aim of this paper is to extend this ceramic processing method to metallic systems, specifically titanium. In the present work, we demonstrate that near-dense and porous titanium structures can be produced by thermoreversible gelcasting of titanium hydride powder. This allows for casting of complex titanium shapes at low temperatures and ambient pressure, thus minimizing contamination and the high processing costs associated with conventional casting of liquid titanium in a high-vacuum, high-temperature environment [1,3,12].

2. Experimental methods

2.1. Materials

The thermoreversible gelcasting system consists of triblock copolymer, solvent, and suspended solids (e.g. titanium hydride particles, organic space-holder). In all experiments, poly(methyl methacrylate)–poly(n-butyl acrylate)–poly(methyl methacrylate) (PMMA–PnBA–PMMA; 23k–31k–23k g mol^{-1}; see Fig. 1) triblock copolymer provided by Kuraray Co. (Japan) was dissolved in 1-pentanol (Alfa Aesar) to a concentration of 7 vol.% copolymer
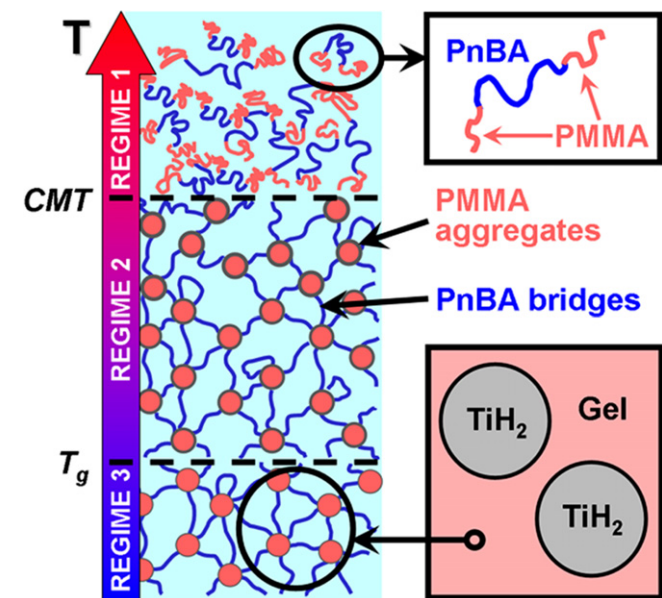

Fig. 1. Schematic representation of the reversible gelation of PMMA–PnBA–PMMA triblock copolymer in solvent with increasing temperature (vertical axis). Regimes 1, 2, and 3 correspond to the low-viscosity liquid, viscoelastic liquid, and elastic solid physical regime, respectively. Micron-sized particles, such as titanium hydride (TiH$_2$) or organic space-holder particles, can be suspended by the gel at room temperature (when the gel is an elastic solid – Regime 3).

unless noted otherwise. For porous titanium fabrication, one of two fugitive space-holders was used: chromatographic grade polypropylene (PP; Polysciences, Inc.) beads and poly(methyl methacrylate) beads (PMMA; Sigma Aldrich) with an average diameter of 35 and 73 ± 20 μm, respectively. Titanium (II) hydride powder (TiH$_2$), 99% pure with a 2 ± 1 μm average particle size (Alfa Aesar) and hydrogen content of 3.9 ± 0.2 wt.% (as determined by Wah Chang Laboratories, Albany, OR, USA), was used as-received for all rheological experiments, PP volume fraction experiments, and for the fabrication of ultrasonic testing samples. For the fabrication of titanium samples used for compression testing and chemical analysis, the fabrication of titanium screws, the investigation of organic pyrolysis with thermogravimetric analysis, and the determination of the hydrogen release temperature with differential scanning calorimetry, –325 mesh titanium hydride powder with a purity of 99.99% and average particle size of 3 μm was used as-received from Alfa Aesar. Hydrogen concentration in the as-received powder was determined to be 4.4 ± 0.2 wt.%, corresponding to TiH$_{2.19}$ (Wah Chang).

2.2. Casting procedure

The triblock copolymer was dissolved in the solvent in a closed vial at 80 °C. Cooling below the gel temperature (∼56 °C) resulted in the formation of an elastic polymer network. Various volume fractions of titanium hydride with and without organic space-holder were added to the vial at room temperature and mixed into a uniform low-viscosity suspension at 75–80 °C using a hot plate and magnetic stirring rod. The heated gel suspension was poured from the vial into heated molds (∼50 °C), consisting of poly(tetrafluoroethylene) flat washers with an inner and outer diameter of 9.6 and 19 mm, respectively, and average height of 4.8 mm (McMaster–Carr, Atlanta, GA, USA). Immediately following casting (within seconds), gelation occurred during cooling in air, effectively suspending all solids. The cylindrical gelled sample was removed from the mold and dried at room temperature in closed and vented pentanol environments, to prevent cracking or warping from rapid solvent evaporation, followed by drying in air. Dried samples could be easily handled due to the triblock copolymer acting as an elastic binder in the system.

2.3. Organic pyrolysis and sintering

Samples contained in alumina crucibles with Ti lids were heat-treated in a vacuum furnace with a nominal low pressure range of 10^{-5}–10^{-6} torr. Heat-treatments consisted of two main stages: (1) a low-temperature dynamic heating stage to remove the triblock copolymer binder and organic space-holder (in the case of porous samples), and to allow for hydride decomposition; and (2) a high-temperature isothermal stage to sinter the tita-

nium particles. Dense titanium resulted from the following heat-treatments: 150–350 °C ramp at 2 °C min^{-1}; 350 °C isothermal hold for 1 h; 350–1000 °C ramp at 7 °C min^{-1}; 1000 °C isothermal hold for 10 h; furnace cool. Porous titanium fabricated with PP and PMMA space-holder followed a similar heat-treatment: 150–375 °C ramp at 2 °C min^{-1}; 375 °C isothermal hold for 0.5–7.5 h (increased hold with greater volume fraction of space-holder); 375–1000 °C ramp at 7 °C min^{-1}; 1000 °C isothermal hold for 10 h; furnace cool.

2.4. Physical and mechanical characterization

Thermogravimetric analysis (TGA) was performed on as-received titanium hydride and dried, gelcast samples in a high-purity argon environment using a Mettler Toledo TGA (model TGA/SDTA851^e). A 2 °C min^{-1} heating rate was employed to simulate the low-temperature organic pyrolysis phase. To determine the onset temperature of hydrogen release from titanium hydride powder, differential scanning calorimetry (DSC) with a Mettler Toledo DSC822^e was performed on as-received powder and a dried, gelcast sample in a high-purity argon environment with standard aluminum crucibles and a heating rate of 10 °C min^{-1} to 600 °C. A Rigaku Geigerflex X-ray Powder Diffractometer with Ni-filtered Cu-K$_\alpha$ radiation, 0.05° step size and 1 s dwell time was used to characterize as-received titanium hydride powder and as-cast titanium hydride samples before and after heat-treatment. Rheological experiments were performed using a stress-controlled rheometer (Paar Physica MCR 300) with a double-gap Couette fixture and Couette Peltier system with cell cover to prevent solvent loss. Steady-state shear viscosity as a function of TiH$_2$ volume fraction in the triblock copolymer gel was investigated over shear rates of 1–1000 s^{-1} at a temperature of 70 °C. Oscillatory temperature sweeps from 70 to 30 °C at a fixed strain of 1% and angular frequency of 10% were performed to determine the gel temperature of the various suspensions.

Closed porosity present in the gelcast samples before and after heat-treating was determined with an AccuPyc 1330 helium pycnometer (Micromeritics Instrument Corp.). Total porosity (obtained via envelope volume) was determined after sintering using the Archimedes method in water with samples sealed with a thin layer of vacuum grease. Open porosity was calculated as the difference between total and closed porosity. Compositional analysis of sintered titanium samples was performed by Wah Chang Laboratories. Sample cross-sections were prepared for scanning electron microscopy (Hitachi S-3400N Variable Pressure SEM, 15 kV accelerating voltage) using standard metallographic techniques and coated with a 5 nm Au/Pd film.

Young's moduli of porous titanium samples were determined using ultrasonic transmission testing with a digital oscilloscope and ultrasonic waves supplied by 5 MHz transducers (Matec Instruments NDT). To minimize scat-

tering effects, transducers were selected such that the signal wavelength was smaller than the sample thicknesses and larger than the pore sizes. Elastic constants were determined from the following equations for longitudinal velocity V_l and shear velocity V_s [39]:

$$V_s = \sqrt{\frac{E}{2\rho(1+v)}} \qquad (1)$$

$$V_l = \sqrt{\frac{E}{\rho}\frac{(1-v)}{(1+v)(1-2v)}} \qquad (2)$$

where ρ is the foam density, v is the foam Poisson's ratio, and E is the foam Young's modulus. Control over sample size ensured a 95% average statistical power to detect a 3 GPa or more departure from the real modulus value; error in ultrasonic evaluation of Young's modulus was estimated to be ±3 GPa due to sample geometry.

Mechanical properties of the porous titanium samples were investigated via compression testing at ambient conditions using a Sintech 20/G testing apparatus (MTS Systems Corporation) at a strain rate of 10^{-3} s^{-1}. Each sample was electric-discharge-machined into a parallelepiped with a height-to-width ratio of 2 (typical dimensions: $2.5 \times 2.5 \times 5$ mm^3). Total porosity of each machined sample was determined by the Archimedes method prior to testing. Strain was determined from cross-head displacement, after correcting for the compliance of the testing apparatus and following calibration with an aluminum standard of known Young's modulus.

3. Results and discussion

3.1. Slurry and casting optimization

Solid particles must remain suspended in the triblock copolymer gel in order to form structurally uniform objects by thermoreversible gelcasting. In prior work, alumina particles with an average diameter of 5 μm were effectively suspended in similar triblock copolymer systems [37]. In order to cast structures from titanium powder (density of 4.5 g cm^{-3}, greater than the density of alumina: 3.9 g cm^{-3}), particles less than 5 μm in diameter are expected to be needed for particle suspension. At this small size scale, the native oxide layer present on the titanium particles would lead to incorporation of a large amount of oxygen into the sintered structure (titanium can dissolve up to 33 at.% oxygen), deleteriously affecting the mechanical properties of the titanium structure [6]. To fabricate titanium structures with reduced oxygen contamination, titanium hydride powder was used instead of titanium powder. Since titanium hydride has a density of 3.9 g cm^{-3}, the powders used in this study with diameters of 1–3 μm were easily suspended. The powder began decomposing into titanium and hydrogen gas at 400 °C (as determined by DSC), thus creating a reducing environment [40–42] further preventing contamination from residual gases.

The following factors were considered when targeting an optimal slurry concentration: (1) strength of the gel, (2) contamination from the copolymer binder, (3) solvent evaporation effects, and (4) linear shrinkage. Decreasing the concentration of copolymer in the gel resulted in a weaker polymer network which fractured upon demolding and warped during solvent evaporation. Increasing the concentration, though adding strength to the gel, resulted in a greater fraction of binder to be pyrolyzed, leading to increased contamination of the sintered sample. It was found that slurry concentrations of 4 vol.% triblock copolymer/35 vol.% solids/61 vol.% pentanol (solids comprising titanium hydride particles and organic space-holder, if present) displayed optimal mechanical properties for casting and sintering.

To minimize linear shrinkage, it is advantageous to increase the volume fraction of solids in the slurry to the maximum value reached when the viscosity of the slurry begins to prohibit quick and uniform molding filling. To characterize slurry viscosity, titanium hydride powder was mixed into a 7 vol.% triblock copolymer/93 vol.% pentanol solution at 70 °C to form slurry concentrations of 0–40 vol.% TiH$_2$ (no space-holder). As shown in Fig. 2, with increasing volume fraction of TiH$_2$ in the slurry, the overall viscosity of the slurry increases. The curves demonstrate behavior typical of particulate suspensions: shear thinning at low shear rates approaching a constant viscosity at higher shear rates (which is a behavior characteristic of a stable, highly concentrated suspension) with shear thickening observed at higher volume fractions [35,43]. The highest volume fraction that could be "gravitationally" cast (poured from the heated vial into a heated mold, with normal atmospheric conditions) was 35 vol.%
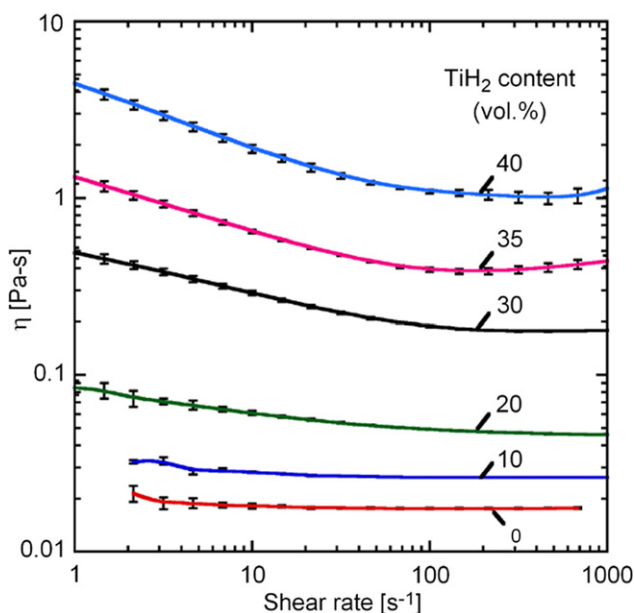

Fig. 2. Steady-state shear viscosity of the gelcasting slurry at 70 °C as a function of TiH$_2$ vol.% in the slurry (no space-holder fraction). Error bars represent one standard deviation of repeated experiments.

TiH$_2$. Slurries with 40 vol.% TiH$_2$, though displaying low-viscosity behavior in the sealed vials, cooled rapidly upon exiting the vial and gelled prematurely (i.e. before filling the mold). This could be prevented by casting in a temperature-controlled, closed environment, such as through a heated and pressurized capillary. The gel temperature (temperature at which the storage and loss moduli intersect [35]) was found to be near 56 °C for all slurry concentrations, confirming that the addition of solids to the polymer network does not affect the reversible gelation behavior.

3.2. Organic pyrolysis and hydrogen evolution

TGA was performed to determine the appropriate low-temperature pyrolysis procedures to remove organics (triblock copolymer and PP or PMMA space-holder) from dried, gelcast samples. The aim was to ensure that pyrolysis would proceed at a sufficiently slow rate to prevent sample cracking or warping, with the majority of organics degraded prior to reaching 400 °C (onset temperature for hydrogen release from TiH$_2$).

As displayed in Fig. 3a, the majority of the triblock copolymer binder was removed from gelcast and dried titanium hydride samples (without space-holder) during the following heat-treatment: 150–350 °C ramp at 2 °C min^{-1}; 350 °C isothermal hold for 60 min. Over 85 wt.% of the binder was removed during the heat-treatment; the remaining organics were expected to decompose during the ramp up to the high-temperature sintering phase. Organic decomposition behavior for PP- and PMMA-filled samples (space-holder content was 30 vol.% of solids) is shown in Fig. 3b during a 150–375 °C ramp at 2 °C min^{-1}. At the end of the heat-treatment, approximately 99 wt.% of the organics present in the PMMA-filled samples were removed by pyrolysis as compared to only 40 wt.% of the organics in the PP-filled samples. With the addition of a 5 h isothermal treatment at 375 °C (not shown), over 90 wt.% of the organics in the PP-filled samples were pyrolyzed.

Evidence of hydride decomposition (an expected 4 wt.% loss) was not observed during any of the above heat-treatments. To ensure hydrogen gas release was not significant at these temperatures, the pyrolysis schedules determined from TGA were repeated in the vacuum furnace with samples of identical compositions, and X-ray diffraction was performed. Spectra obtained before and after the heat-treatments were alike for all samples, indicating that the titanium hydride powder did not decompose.

The difference in pyrolysis behavior for the PP- and PMMA-filled samples is due to the disparity in degradation mechanisms of these polymers. TGA experiments performed on PMMA and PP homopolymer in a nitrogen environment (not shown here) displayed a maximum degradation rate at 380 and 450 °C, respectively. The greater thermal stability of PP compared to PMMA is due to the structures of the polymers. PMMA begins to degrade at temperatures as low as 250 °C via depolymerization,
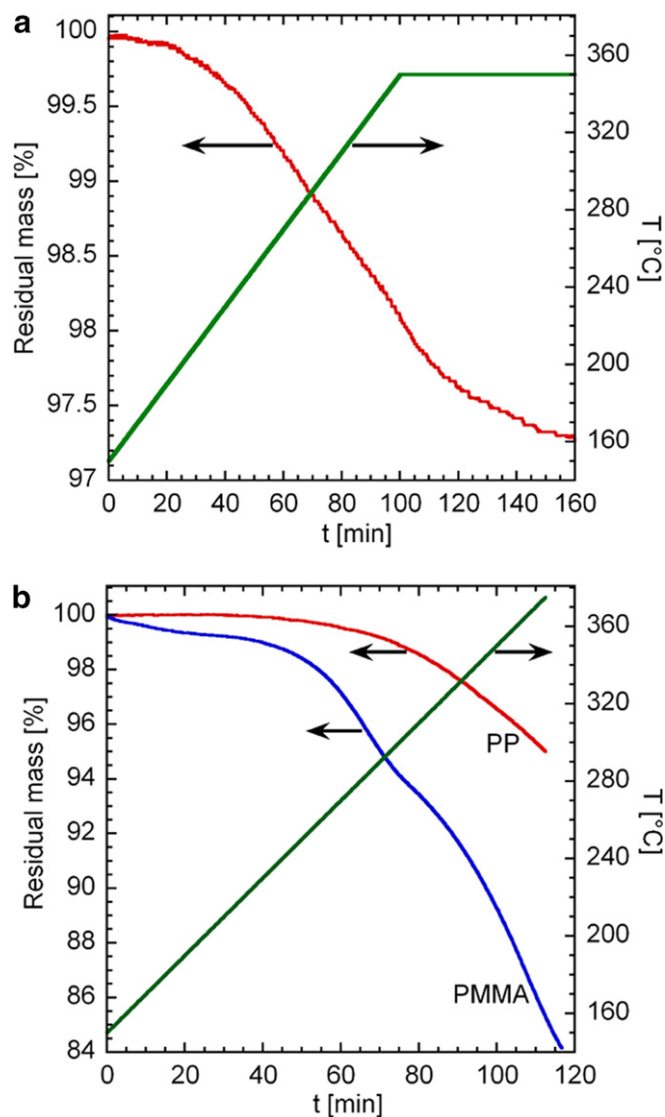

Fig. 3. Residual mass (by TGA; left axis) from degradation of organic components as a function of time during controlled heating (right axis) of a dried, gelcast titanium hydride sample (a) without organic space-holder (triblock copolymer binder only) and (b) with the addition of 30 vol.% PP or PMMA space-holder.

whereas PP begins to degrade at ~360 °C by random chain scission [44].

3.3. Thermoreversible gelcasting and sintering

To confirm the dependence of Ti foam density on volume fraction of organic space-holder, slurry concentrations of 4 vol.% triblock copolymer/35 vol.% solids (TiH$_2$ + PP)/61 vol.% pentanol were gelcast, dried, and heat-treated. The amount of PP space-holder in the slurry was varied from 0 to 50 vol.% of the solids (i.e. excluding the triblock copolymer binder and the solvent). As expected, total porosity of the sintered Ti samples was observed to increase with PP volume fraction and transition from predominantly closed to open porosity (Fig. 4). The dashed
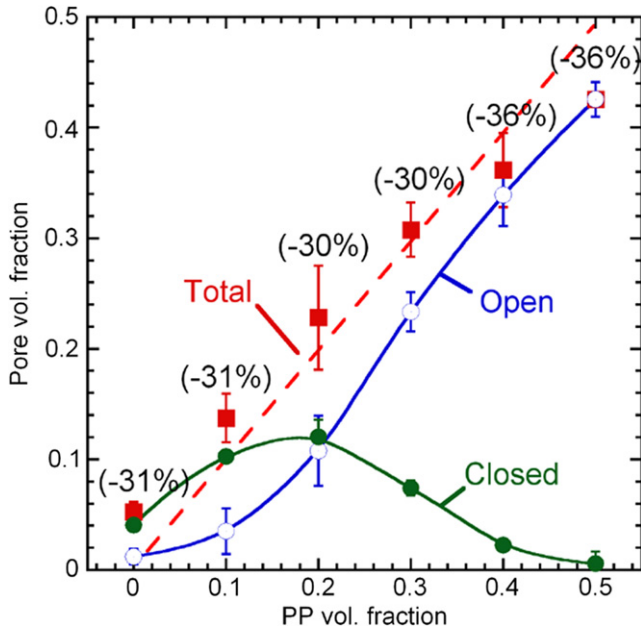
Fig. 4. Open, closed, and total pore volume fraction of gelcast and sintered Ti foams as a function of PP space-holder volume fraction. Average linear shrinkage of the foams is indicated in parentheses. Error bars indicate the 90% confidence intervals for the measured porosity.

line in Fig. 3 corresponds to the extreme case where small pores between the metal particles disappear completely by sintering while the volume of the larger pores from the PP space-holder remains unchanged (e.g. 20 vol.% porosity expected for 20 vol.% PP). Total porosity is slightly inflated from the extreme case due to the 4 vol.% porosity which forms from incomplete densification of the TiH$_2$ powder. At PP concentrations of 0 vol.% and 10 vol.%, which are below the percolation limit, the open porosity most probably corresponded to surface pores resulting from trapped air bubbles during casting as well as surface roughness of the dried samples. At and above 40 vol.% PP, total porosity was slightly less than expected (e.g. addition of 50 vol.% PP only yields 42 vol.% porosity). This effect was due to increased densification of the open porous structure, confirmed by the increase in isotropic linear shrinkage of the samples (given in parentheses in Fig. 4). The fraction of closed porosity present in the 50 vol.% PP sample was below the resolution of the pycnometer (<1 vol.% porosity).

Two types of porosity were present in the sintered samples (Fig. 5a–f). Irregular porosity attributed to PP space-holder generally ranged in size from 30 to 50 μm, with size scale and morphology similar to the space-holder particles (larger pores are due to agglomeration of PP). Near-spherical porosity less than 5 μm in size was observed near the surfaces of the 0 vol.% PP samples (inset of Fig. 5a) and 10 vol.% PP samples. The majority of near-spherical porosity in the 0 vol.% PP sample was within approximately 20 μm of the sample surface after sintering. Similar interior-to-surface porosity gradients were observed in pow-

der-injection-molded titanium when solvent and binder removal were performed [45] and were partly attributed to the creation of pore channels in the sample that allow for solvent evaporation from the bulk as well as volatile transport during pyrolysis [29]. Solvent in the bulk of the sample must diffuse and evaporate at the surface. During sintering, densification of the samples effectively closes the smaller, internal channels while the larger channels near the surface remain.

Chemical analysis was performed on sintered titanium samples that were gelcast from slurries with and without organic space-holder (Table 1). For the two samples initially containing 30 vol.% space-holder, a lower carbon content was found in the sample fabricated with PMMA. This is because PMMA begins degrading at a lower temperature and degrades more rapidly during the pyrolysis step, as seen from the TGA results (Fig. 3b), limiting any reaction with TiH$_2$. As expected, the carbon content was lowest for the sample without space-holder. Oxygen content for all samples increased modestly, from 0.24 wt.% for the as-received titanium hydride powder to 0.60–0.70 wt.% for the sintered samples. As expected from vacuum sintering, hydrogen concentrations were very low (Table 1).

3.4. Ultrasonic measurement of foam stiffness

Young's modulus values for gelcast and sintered Ti samples determined by ultrasonic testing were found to vary inversely with porosity (Fig. 6). Results from the current work (filled symbols) are plotted with reported values for Ti foams produced by various processing routes: solid-state gas foamed Ti [46], Ti fabricated with magnesium powder as space-holders [17], and partially sintered Ti [14]. Open symbols denote moduli determined from compression testing stress–strain curves while the filled symbols are ultrasonic values. The present gelcast and sintered Ti samples exhibit the highest moduli at a given relative density, indicative of complete sintering of the titanium matrix. Young's modulus values measured here are in good agreement with values predicted by the Gibson and Ashby model for open cellular materials [47]:

$$\frac{E}{E_o} = \left(\frac{\rho}{\rho_o}\right)^n \tag{3}$$

where E and E_o are Young's moduli of the foam and fully dense Ti (120 GPa [3]), ρ and ρ_o are the densities of porous and bulk Ti (4.51 g cm^{-3} [3]), and n has a value between 1.8 and 2.2 [48]. The scaling exponent used here, $n = 1.8$, is within the acceptable range for metal foams but somewhat below the commonly accepted value of 2. A more rigorous model based on the Mori–Tanaka composite approach was developed by Zhao et al. [49] for isolated, spherical voids with zero stiffness in an elastic matrix; this approach coincides with the Hashin–Shtrikman upper bound. The model is applied here following Ref. [46] with a Poisson's ratio $v = 0.361$, bulk elastic modulus $K_o = 147$ GPa, and a shear
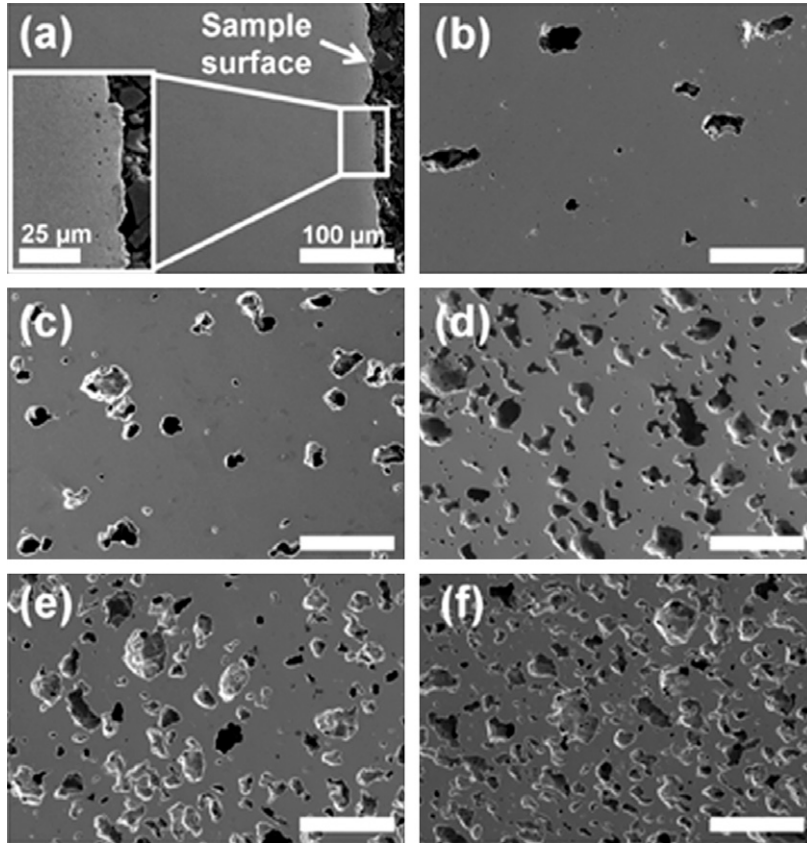
Fig. 5. SEM images of cross-sections of gelcast and sintered Ti foams initially containing various PP volume fraction (corresponding to Fig. 4): (a) 0 vol.%, (b) 10 vol.%, (c) 20 vol.%, (d) 30 vol.%, (e) 40 vol.%, and (f) 50 vol.%. All images are at the same magnification, except for inset in (a).

Table 1
Chemical analysis (wt.%) of as-received titanium hydride powder and sintered Ti bulk samples

Sample	Hydrogen	Oxygen	Carbon
TiH$_2$ powder (as-received)	4.4	0.24	–
Ti (no space-holder)	0.0054	0.60	0.14
Ti (30 vol.% PP)	0.024	0.70	0.73
Ti (30 vol.% PMMA)	0.011	0.71	0.66

modulus value $\mu_o = 44$ GPa [3]. This model is very close to the Gibson–Ashby model (Eq. (3)), despite the fact that the latter model was derived for cellular structures with relative density typically below 0.3.

3.5. Compression testing of Ti foams

Mechanical testing was performed on gelcast and sintered Ti samples with low and high levels of porosity, 4 vol.% and 36–41 vol.%, fabricated from gelcasting slurries containing 0 and 30 vol.% space-holder, respectively (see Table 2). Compared to the porosity percentages reported in Fig. 4 as a function of PP volume fraction, greater porosity was observed in the Ti samples used for mechanical testing at equivalent space-holder volume fractions. This porosity increase is related to the use of low-oxygen titanium hydride powder (–325 mesh, corresponding to
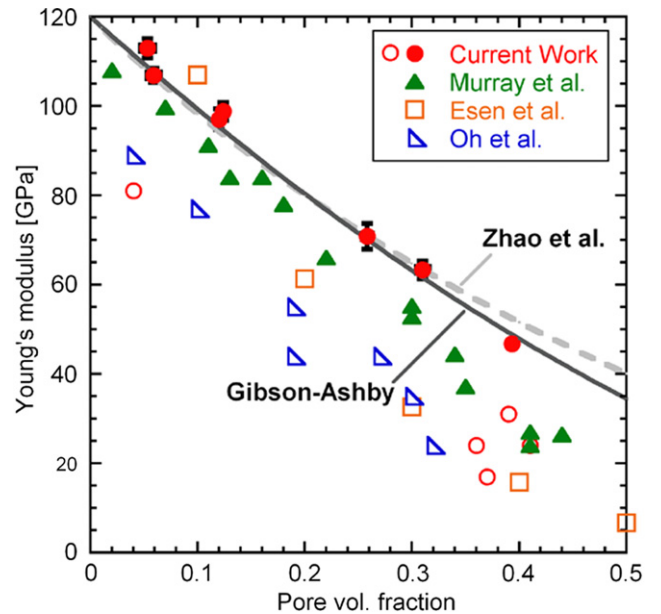

Fig. 6. Young's moduli determined from ultrasonic testing (filled symbols) and compression testing (open symbols) as a function of Ti porosity. Error bars (often smaller than the data points) indicate 95% confidence intervals for porosity (determined by Archimedes method) and for Young's modulus. Literature values are displayed for various foams (processing described in the text), measured ultrasonically for Murray et al. [46] and from stress–strain curves for Esen et al. [17] and Oh et al. [14].

Table 2
Porosity and mechanical properties determined from compression testing of sintered Ti samples

Space-holder content	Post-sintering porosity[a] (vol.%)	Stiffness (GPa)	0.2% Yield stress (MPa)
0 vol.%	4[b]	81[b]	445[b]
30 vol.% PP	36	24	200
	37	17	213
30 vol.% PMMA	39	31	200
	41	24	171

[a] Open porosity, except for sample without space-holder.
[b] Average of two samples.

particle diameters <44 μm) for the compression testing samples compared to the 1–3 μm powder used previously in this study. Larger titanium hydride particles resulted in less-efficient packing around the space-holder particles. The microstructure of the samples was similar to Fig. 5e with pore size ranging from 30 to 50 μm for PP space-holder and 50 to 70 μm for the larger PMMA space-holder. The corresponding compressive stress–strain curves are shown in Fig. 7, with quantitative results summarized in Table 2.

Chemical analysis performed on the two 4 vol.% porous Ti samples after compression testing resulted in oxygen concentrations of 0.45 wt.%. This is below the value of 0.60 wt.% oxygen measured from the bulk sample (Table 1), indicative of an oxygen concentration gradient from the interior of the bulk sample (from which the compression testing sample was machined) to the exterior region of the sample (subjected to longer exposure to the escaping gases during pyrolysis). Thus, the 4 vol.% porous compres-

sion samples have oxygen concentrations only slightly higher than Grade 4 commercially pure Ti (0.4 wt.% oxygen). In compression, dense Grade 4 Ti samples were reported to exhibit a 0.2% offset yield strength of ~550 MPa at room temperature [50]. The gelcast samples displayed lower yield stress values (445 MPa, Table 2) most likely due to the 4 vol.% closed porosity incorporated in the structure and/or larger grain size due to different processing route and heat-treatment. Compared with a Grade 2 dense Ti compressive curve (0.25 wt.% oxygen; cold drawn and annealed) shown in Fig. 7, the 4 vol.% porous Ti curves exhibited greater strength and strain hardening, as expected from the higher oxygen content [51,52].

The smooth stress–strain curves of the high-porosity Ti samples (Fig. 7) are characteristic of ductile metallic foams with equiaxed uniform porosity: the initial linear elastic region (resulting from bending cell walls) transitions into a plastic plateau region (characteristic of cell collapse) followed by densification [47]. Oxygen content of these samples was found to be ~0.6 wt.% – a significant decrease from the values reported in Table 1 for the bulk samples – thus confirming the existence of an oxygen contamination gradient. A compressive stress–strain curve of 41 vol.% porous Grade 2 Ti produced by solid-state foaming [20] is plotted in Fig. 7 (dashed curve) for comparison. The present Ti foams produced by thermoreversible gelcasting displayed improved strength and energy absorption (area under the stress–strain curve). The greater strain hardening of the present foams was also expected from their greater oxygen content as compared to the 41 vol.% porous Grade 2 result [52].

The stiffness values determined from the initial linear region of the compressive stress–strain curves (reported in Table 2 and plotted in Fig. 6) were significantly lower than those obtained from ultrasonic testing. Ultrasonic testing provides more reliable elastic modulus values than compression testing: local microplasticity at very low strain levels in compression testing can result in near-linear stress–strain slopes that are much lower than the true Young's modulus [47,53]. In fact, many of the literature values plotted in Fig. 6 were measured on stress–strain curves, which can partially explain their low values as compared to the present foams and the model predictions.

Yield stress values determined from the 0.2% offset from the compression stress–strain curves are reported in Table 2. Compressive strength of metallic foams can be predicted using the Gibson and Ashby model for open cellular materials:

$$\frac{\sigma}{\sigma_s} = C\left(\frac{\rho}{\rho_s}\right)^{3/2} \qquad (4)$$

where σ and σ_s denote the strength of the porous and dense metal and C is a scaling factor typically near 0.3, but which can range from 0.1 to 1 [48]. Using a compressive strength $\sigma_s = 760$ MPa (as reported for dense Ti with 0.6 wt.% oxygen [54]), Eq. (4) is best fit to the data for $C = 0.53$
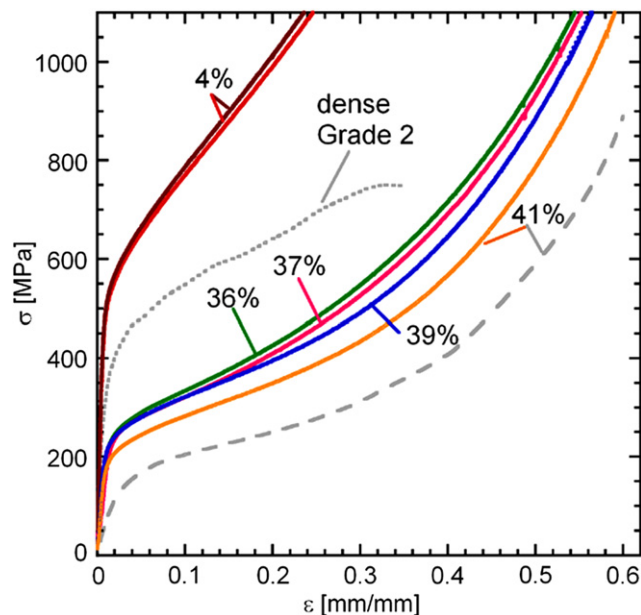

Fig. 7. Compressive stress–strain curves of gelcast and sintered Ti samples with varying levels of porosity (indicated next to curves). The dashed compressive curve from 41% porous Ti is from Ref. [20]. The dense Grade 2 Ti dotted compressive curve is from Ref. [51].

indicating that the foams have good strength. The porosity range of 36–41% is too narrow to draw further conclusions, but it is noteworthy that a scaling constant value greater than 0.3 was expected from microcellular modeling performed by Despois et al. [55].

Overall, ultrasonic and compression tests confirm the ability of thermoreversible gelcasting to produce porous titanium with excellent compressive stiffness, strength, ductility, and energy absorption characteristics.

3.6. Technological implications and complex titanium shapes

Besides the advantages outlined previously of thermoreversible gelcasting compared to conventional gelcasting, additional benefits are realized when fabricating titanium structures. Water is a primary component of conventional gelcasting systems developed previously for metal powders [29]. Fine titanium powder is expected to be severely oxidized by water, with the oxygen present in solid solution in the titanium after high-temperature powder densification [6]. The thermoreversible gelcasting process described here relies on a non-aqueous system as the powder transport medium, thereby eliminating an important source of oxygen contamination. A non-aqueous system also allows for the use of titanium hydride powder (which would react strongly with water) and subsequent creation of a reducing environment during decomposition to metallic titanium. Finally, the most unique characteristic of thermoreversible gelcasting is the temperature-dependent, reversible gelation process, allowing multiple casting attempts if casting irregularities occur without creating additional material waste.

To demonstrate the ability to cast complex shapes, porous screws (Fig. 8) were gelcast from a 6 vol.% copolymer/ 7 vol.% PP/28 vol.% titanium hydride/59 vol.% pentanol slurry using silicone molds of steel screws 19.1 mm in length. Concentration of the thermoreversible gel was increased to 10 vol.% copolymer to provide additional strength to the gelled structure and prevent warping during drying. After heat-treating, porosity within approximately 200 μm of the surface (determined to range from 30 to 35 vol.% by image analysis) had an angular, jagged appearance compared to the pore morphology in the interior of the screw which was similar in appearance and fraction to Fig. 5c for 20 vol.% space-holder. The interior porosity resulted from pyrolysis of PP space-holder (which accounted for 20 vol.% of solids) whereas the angular open porosity near the surface is believed to result from damage incurred by the gel matrix during demolding that was only partially healed during drying and sintering of the screw. This dense-core/porous-surface structure, arrived at through the unique elastic properties of the thermoreversible gel, is desirable for biomedical implants where fully porous metal may not provide sufficient strength (e.g. for highly stressed dental implants and joint arthroplasty implants). Screws with such a gradient in porosity benefit from good mechanical anchoring via bone ingrowth without sacrificing the strength of the denser core [5].
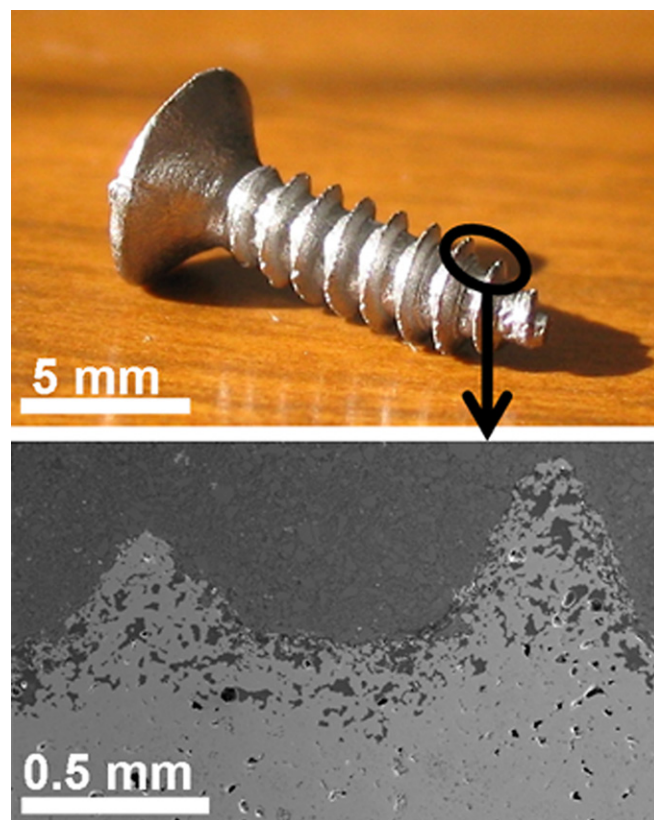

Fig. 8. Photograph and SEM cross-sectional micrograph of gelcast and sintered Ti screw with a 20 vol.% porous core and enhanced porosity near the surface. Greater contrast of the porosity near the surface is due to bakelite infiltration.

In addition to fabricating complex titanium shapes through a simple casting technique as demonstrated here, thermoreversible gelcasting can be easily adapted for use with existing powder injection molding technology [56]. Utilizing plastic injection molding machines, metal and ceramic components can be produced by heat-treating an injection-molded shape composed of organic binder and metal or ceramic powder. Incorporation of the thermally reversible gel studied here as the binder would allow feedstock mixing and injection molding to take place at temperatures less than 70 °C and pressures of the order of 1 MPa [56] afforded by the low viscosities demonstrated here at 70 °C (Fig. 2). Low temperatures and pressures are advantageous when working with reactive metals such as titanium, compared to temperatures of 85–275 °C and pressures of 20–60 MPa that have been used previously to injection-mold titanium [45,57] and $TiAl_6Nb_7$ [58].

4. Summary

Thermoreversible gelcasting, originally developed as a ceramic processing technique, has been successfully utilized for the fabrication of porous titanium structures. The gelcasting system is composed of titanium hydride particles,

with and without organic space-holders to produce porosity, suspended in a thermally reversible, physically crosslinked triblock copolymer gel that acts as a liquid transport medium above 56 °C and an elastic solid at room temperature. Organic pyrolysis to remove the gel and space-holder followed by vacuum sintering to densify the Ti powders produced by decomposition of the hydride results in titanium foams. With control over slurry rheological properties, thermoreversible gelcasting of Ti could be combined with powder injection molding technology to develop a low temperature and pressure molding system. The main conclusions are as follows:

(1) Oxygen and carbon contamination are minimized through the use of pentanol instead of water as solvent, titanium hydride in place of metallic titanium, and organic space-holders (PP and PMMA) that degrade at temperatures below the decomposition of titanium hydride.

(2) Incorporation of PP and PMMA organic space-holders result in titanium with controlled porosity ranging from 4 to 44 vol.% which displays greater stiffness-to-weight ratios than porous titanium fabricated by other processes. The compressive stress–strain curves are typical of metallic foams having equiaxed uniform porosity; the foams display good strength, ductility, and energy absorption.

(3) To demonstrate the net-shape forming capability of thermoreversible gelcasting, a titanium screw is created which exhibits a porous surface and a relatively dense core. This graded structure is useful for medical implants.

Acknowledgements

References

[1] Dunand DC. Adv Eng Mater 2004;6:369.
[2] Brunette DM, Tengvall P, Textor M, Thomsen P. Titanium in medicine: material science, surface science, engineering, biological responses, and medical applications. Berlin, New York: Springer Verlag; 2001.
[3] Donachie MJ. Titanium: a technical guide. Materials Park, OH: ASM International; 2000.
[4] Pohler OEM. Injury – Int J Care Injured 2000;31 :S7.
[5] Ryan G, Pandit A, Apatsidis DP. Biomaterials 2006;27:2651.
[6] Leyens C, Peters M. Titanium and titanium alloys: fundamentals and applications. Weinheim, Chichester: Wiley-VCH; 2003.
[7] Rak ZS, Walter J. J Mater Process Technol 2006;175:358.
[8] Saupe GB, Zhao Y, Bang J, Yesu NR, Carballo GA, Ordonez R, et al. Microchem J 2005;81:156.
[9] Banhart J. Prog Mater Sci 2001;46:559.
[10] Lu G, Yu TX. Energy absorption of structures and materials. Cambridge: Woodhead; 2003.
[11] Gauthier M, Lefebvre LP, Thomas Y, Bureau MN. Mater Manuf Process 2004;19:793.
[12] Chen CC. Recent advancements in titanium near-net-shape technology. In: Hasson DF, Hamilton CH, editors. TMS fall meeting. Louisville, KY. Berlin: Springer; 1981. p. 3.
[13] Thieme M, Wieters KP, Bergner F, Scharnweber D, Worch H, Ndop J, et al. J Mater Sci – Mater Med 2001;12:225.
[14] Oh IH, Nomura N, Masahashi N, Hanada S. Scripta Mater 2003;49:1197.
[15] Laptev A, Bram M, Buchkremer HP, Stover D. Powder Metall 2004;47:85.
[16] Bram M, Stiller C, Buchkremer HP, Stover D, Baur H. Adv Eng Mater 2000;2:196.
[17] Esen Z, Bor S. Scripta Mater 2007;56:341.
[18] Wen CE, Yamada Y, Shimojima K, Chino Y, Asahina T, Mabuchi M. J Mater Sci – Mater Med 2002;13:397.
[19] Chino Y, Dunand DC. Acta Mater 2008;56:105.
[20] Davis NG, Teisen J, Schuh C, Dunand DC. J Mater Res 2001;16:1508.
[21] Ricceri R, Matteazzi P. Int J Powder Metall 2003;39:53.
[22] Laptev A, Vyal O, Bram M, Buchkremer HP, Stover D. Powder Metall 2005;48:358.
[23] Young AC, Omatete OO, Janney MA, Menchhofer PA. J Am Ceram Soc 1991;74:612.
[24] Omatete OO, Janney MA, Strehlow RA. Am Ceram Soc Bull 1991;70:1641.
[25] Dong DH, Gao JF, Liu XQ, Meng GY. J Power Sources 2007;165:217.
[26] Chen WW, Kinemuchi Y, Tamura T, Miwa K, Watari K. J Eur Ceram Soc 2007;27:655.
[27] Ganesh I, Jana DC, Shaik S, Thiyagarajan N. J Am Ceram Soc 2006;89:3056.
[28] Janney MA, Omatete OO, Walls CA, Nunn SD, Ogle RJ, Westmoreland G. J Am Ceram Soc 1998;81:581.
[29] Janney MA. In: Froes FH, editor. Fourth international conference on powder metallurgy in aerospace defense and demanding applications. Anahein, CA: Metal Powder Industries Federation; 1995. p. 139.
[30] Janney MA, Ren W, Viswanathan S. Adv Powder Metall Particul Mater 1997;5:227.
[31] Li Y, Guo Z, Hao J. J Univ Sci Technol Beijing 2007;14:507.
[32] Liu WH, Jia CC, Shi YT, Han YP. Rare Metals 2008;27:78.
[33] Drzal PL, Shull KR. Macromolecules 2003;36:2000.
[34] Seitz ME, Burghardt WR, Faber KT, Shull KR. Macromolecules 2007;40:1218.
[35] Larson RG. The structure and rheology of complex fluids. New York: Oxford University Press; 1999.
[36] Drzal PL, Shull KR. Eur Phys J E 2005;17:477.
[37] Montgomery JK, Drzal PL, Shull KR, Faber KT. J Am Ceram Soc 2002;85:1164.
[38] Montgomery JK, Botha AS, Drzal PL, Shull KR, Faber KT. Scripta Mater 2003;48:785.
[39] Henneke E. I. Ultrasonic wave propagation. In: Moore PO, editor. Nondestructive testing handbook: ultrasonic testing, vol. 7. Columbus, OH: American Society for Nondestructive Testing; 2007.
[40] Matijasevic-Lux B, Banhart J, Fiechter S, Gorke O, Wanderka N. Acta Mater 2006;54:1887.
[41] Sandim HRZ, Morante BV, Suzuki PA. Mater Res 2005;8:293.
[42] Kennedy AR. Scripta Mater 2002;47:763.
[43] Bergstrom L, Sjostrom E. J Eur Ceram Soc 1999;19:2117.
[44] Kelen T. Polymer degradation. New York: Van Nostrand Reinhold; 1983.
[45] Simmons KL, Scott Weil K, Hyberg EA, Miller M. Powder injection molding of titanium components. Medical device materials II. In: Proceedings of the materials and processes for medical devices conference, 2004, St Paul, MN. Materials Park, OH: ASM International; 2005. p. 229.
[46] Murray NGD, Dunand DC. J Mater Res 2006;21:1175.

[47] Gibson LJ, Ashby MF. Cellular solids: structure and properties. New York: Cambridge University Press; 1997.

[48] Ashby MF, Evans A, Fleck NA, Gibson LJ, Hutchinson JW, Wadley HNG. Metal foams: a design guide. Boston, MA: Butterworth-Heinemann; 2000.

[49] Zhao YH, Tandon GP, Weng GJ. Acta Mech 1989;76:105.

[50] Welsch G, Boyer R, Collings EW. Materials properties handbook: titanium alloys. Materials Park, OH: ASM International; 1994.

[51] Stanford N, Carlson U, Barnett MR. Metall Mater Trans A – Phys Metall Mater Sci 2008;39A:934.

[52] Conrad H. Prog Mater Sci 1981;26:123.

[53] Thelen S, Barthelat F, Brinson LC. J Biomed Mater Res A 2004;69A:601.

[54] Donachie MJ. Titanium: a technical guide. Metals Park, OH: ASM International; 1988.

[55] Despois JF, Mueller R, Mortensen A. Acta Mater 2006;54:4129.

[56] Goncalves AC. J Mater Process Technol 2001;118:193.

[57] Weil KS, Nyberg EA, Simmons KL. Mater Trans 2005;46:1525.

[58] Aust E, Limberg W, Gerling R, Oger B, Ebel T. Adv Eng Mater 2006;8:365.